Fuel 317 (2022) 123196

Contents lists available at ScienceDirect

Fuel

journal homepage: www.elsevier.com/locate/fuel

Full length article

Study of the hydraulic characteristics of two injectors fed with different fuels in a GDI system

Raul Payri *, Jaime Gimeno, Pedro Marti-Aldaravi, Victor Mendoza Alvarez

CMT - Motores Térmicos, Universitat Politècnica de València, Edificio 6D, 46022, Valencia, Spain

ARTICLE INFO

Keywords:
GDI
Nozzle flow
Gasoline surrogates
e-fuels
Mass flow rate
Momentum flux

ABSTRACT

In the latter years, the Gasoline Direct Injection systems (GDI) have been studied with the aim of providing a solution to the particulate matter emission issue. It has been proved that emission levels are reduced with the tuning of certain variables, such as the injection pressure, that affect the internal flow in the nozzle, which in turn plays an vital role in the spray development. On the other hand, the implementation of fuels such as alcohols and some surrogates shows potential for improving the engine performance and emissions because of the different physical properties of the fuels that can alter the mixture formation and the chemical properties that affect the combustion. In this work, an experimental study of the influence of different fuels on the internal flow is realized for a vast number of conditions, including those that promote flash boiling and strong collapse of the spray at different ambient temperatures and pressures. The fuels employed are three components of gasoline: iso-octane, n-hexane and n-pentane; ethanol; and two blends (E00 and E20) for two nozzle geometries. Two experimental techniques are used to measure the mass flow rate and momentum flux of the spray, and then characterize the flow inside the nozzle. The results show a similar injector behavior for all fuels, except for the ethanol, which shows an increase in the rate of injection and induces a hydraulic delay.

1. Introduction

In recent years the interest in new injection technologies and the improvement of the existing ones have maintained the intention of broadening the understanding of this complex process due to its implications in the engine performance. An area that has received special attention is the Direct Injection Spark Ignition (DISI) engines since they provide a potential alternative in the short-medium term for the light automotive sector for improving the brake-specific fuel consumption, volumetric efficiency, lowering the NOx emissions thanks to the possibilities of achieving the combustion with a homogeneous air–fuel mixture at relative low temperatures (during high load and high speed), and competing with Diesel engines with relation to CO emissions [1–3]. This point is not minor since passenger cars, light trucks, and vans, among other daily used light vehicles account for about a third of global oil demand and produce nearly half of all transportation-related greenhouse gas emissions as per 2021 International Council on Clean Transportation (ICCT) report [4].

The emission reduction in car engines has been subject to multiple investigations due to its impact on the ambient; even though the tendency is a shift to electric vehicles, there are still some concerns about the extent of its applicability in the middle term. Thus, the improvement in the automotive research area is required not only for this type of vehicle but also for some hybrid applications that are capturing more space in the market.

DISI engines give important advantages relative to Port Fuel Injection (PFI) engines like lower fuel consumption, better fuel metering, higher efficiency, and low CO_2 emissions [5,6]. Still, they present problems with particle number emissions (PN). In GDI engines, the particle formation is controlled by the air–fuel mixture formation [7]. Thus, an incomplete evaporation mixture leads to PN emissions. A solution that has been shown to improve this matter is increasing the injection pressure, as stated by Raza et al. [7], Lee and Park [8]. This variable has increased progressively in state of the art to the point that nowadays, they can work up to 35 MPa. There exist some cases in hybrid engines where they can reach up to 80 MPa [9], showing to have a positive effect reducing particle number by reducing tip wetting and minimizing fuel wall films inside the combustion chamber [6]. Furthermore, the injection pressure impacts the combustion characteristics, and increasing it produces smaller particles due to better atomization, which enhances the air–fuel mixture process, since large diameter droplets are difficult to get fully evaporated before ignition start [10]. Another interest of GDI engines is that they have NOx emissions similar to those of PFI

* Corresponding author.
E-mail address: rpayri@mot.upv.es (R. Payri).

https://doi.org/10.1016/j.fuel.2022.123196
Received 31 October 2021; Received in revised form 17 December 2021; Accepted 8 January 2022
Available online 5 February 2022

Nomenclature

The following abbreviations are used in this manuscript:

CFD	Computer fluid dynamics.
DISI	Direct injection spark ignition
ECN	Engine Combustion Network.
ECU	Engine Control Unit.
EGR	Exhaust Gas Recirculation.
GDI	Gasoline Direct Injection.
PN	Particulate number.
ROI	Rate of injection.
ROM	Rate of momentum.
SOE	Start of energizing.
SOI	Start of injection.

and depict a severe reduction relative to Diesel engines [2,11,12]. This effect happens due to the fuel evaporation aiding to cool the fuel–air mixture and reduce the combustion temperature. Nonetheless, with the injection pressure increase tendency, this GDI benefit might suffer some drawbacks since higher pressures promote faster and more complete combustion, which increases the ambient temperature [13]. Albeit CO2 emissions are still a pending task, there are other tools as EGR and hybridization that seem promising for the recent future to simultaneously reduce these emissions keeping the gains given by the GDI systems [11].

Another solution that is gaining field for this problem is taking advantage of processes occurring with this type of injection, such as flash boiling. Flash boiling is a spray formation process that is distinguished by smaller droplet mean diameter, higher homogeneity, wider cone angle and shorter penetration depth in an isolated spray plume for the same operating pressure [14]. In the same sense, the intentional use of flash boiling has been discussed as a strategy to increase fuel–air mixing rates and reduce spray impingement on engine cylinders. This phenomenon happens when the ambient temperature is above the boiling point of the most volatile fuel components at the cylinder pressure (or pressure below the saturation pressure) [15]. However, for some conditions, the flash boiling leads to the collapse of the spray plumes into a single extended one with longer spray penetration compared to a standard injection [16]. The collapse depends not only on the operating conditions but also on the fuel properties as it was found by Aleiferis and Van Romunde [17] when comparing ethanol and butanol, as well as, it has been reported by other authors [5,18].

In this context, the influence of fuels is also a subject of interest; however, the properties of traditional gasoline used in engines vary depending on its source, and the production process [19,20]. For this reason, researchers usually use some standardized mixtures that can emulate the gasoline behavior, or that are an important portion of the substances that compound the gasoline and yet conserve the physical and chemical characteristics, such as ignition delay time, burning velocity, viscosity, vaporization, and emissions [21]. The typical commercial gasoline is compound by several hydrocarbons outstanding alkanes, isoalkanes, and aromatics, with carbon atoms going from C5 to C8, and some remainder C9–C10 hydrocarbon chains [20] which implies that surrogates of gasoline could have five to eight carbon atoms [21].

On the other hand, alcohols have also been investigated as gasoline substitutes thanks to the reported benefits on the combustion process [22–24]. Several authors have already studied the influence of alcohols in blends [5,23,25–27], they have found that the ethanol or other alcohol addition into gasoline exhibits anti-knock behavior, improves combustion efficiency, in-cylinder pressure, fuel consumption, reduces CO emissions, promotes a reduction in particulate emissions for specific conditions, and acts as an octane enhancer. Additionally, combining these blends with flash boiling conditions reduces the PN emissions. Further, owing to bioethanol's oxygen content, better particulate matter oxidation is reached, reducing these emissions up to 78.9%.

Gasoline direct injection (GDI) systems can help reduce pollutant emissions by precisely adjusting the time the fuel is injected. The most significant parameter essential to this aim is the mass flow rate, which, combined with the spray momentum, give an indirect characterization of the internal flow in the injector. Moreover, these variables determine the amount of energy which is carried by the fuel jet [28].

The rate of momentum and injection (ROM and ROI) are measurements that have been deeply researched in Diesel engines due to their influence on the combustion process. Yet, several investigations are still being carried out. However, due to the novelty of the GDI technology at relatively high injection pressures (still one order of magnitude inferior to Diesel systems), most of the data available in the literature corresponds to direct injection compression ignition.

In the latter years, some experimental and numerical investigations have been developed on the indirect measurement of the internal flow. For instance, Cavicchi et al. [29] performed CFD (Computational Fluid Dynamics) numerical simulations to model the spray momentum measurement of a single hole GDI spray for n-heptane and 100 bar of injection pressure. They also studied different parameters that affect the force method for obtaining the momentum flux. Mohapatra et al. [30], on their behalf, collect a group of models that have been able to accurately predict the mass flow rate for a specific GDI injector as the work carried out by Shahangian et al. [31]; however, these models need to be tested with newer data with multiple conditions. Additionally, they state that models to predict the external spray details under various conditions are not easy to develop. In this sense, some models to simulate the spray plumes have been successfully done for certain operating conditions, such as Di Ilio et al. [32] who succeed in reproducing the main features of a multi-hole GDI injector.

In this work, three gasoline surrogates, one alcohol, two blends; one between different gasoline pure components, and another adding ethanol are studied for two injectors capable of reaching 20 and 35 MPa, at different conditions, to measure the ROI and ROM. The conditions presented in this work serve as an essential basis for further studies and other types of experiments with these types of fuels, thanks to the utilization of high injection pressures, which are the most critical variable for the spray characteristics. Additionally, new data for these variables at higher injection pressure in GDI injectors is provided. The mass flow rate and momentum flux, apart from providing good information of the internal flow behavior of the injectors, are indispensable for numerical CFD.

Following this introduction, the next section describes the tools, facilities, and experimental techniques used. Later the results and analysis section and finally, the conclusions.

2. Materials and methods

2.1. Injectors and injection conditions

Two solenoid multi-hole injectors with different geometry from two other manufacturers were used to measure the mass flow rate and rate of momentum with different fuels. The injectors can operate at different injection pressures. The injectors' main characteristics are shown in Table 1.

The first injector was donated by Delphi to the Engine Combustion Network (ECN) for research purposes, and the second is a Continental manufactured conventional GDI injector. The first, with AV67-026 serial number, is an injector that has been widely used in the ECN and is labeled as "Spray G" for comparability effects with other parallel research works. The second is marked as C3536. Additionally, the C3539 injector possesses a higher volume in the fuel inlet, which works as a "mini rail", helping to mitigate the changes in the injection pressure. Both were driven by its particular engine control unit (ECU)

Table 1
Injector properties.

Parameter	Spray G	C3539	Units
Holes	8	6	–
Max. pressure	240	350	bar
Orifice diameter $\bar{D}o$	165	146	μm
Orifice length	160–180	400	μm
Spray angle	80	70	°
Orifice type	Step hole	Cylindrical	–
Spray shape	Circular	Circular	–

*Lengths of inner and outer diameters.

provided by the manufacturer with their preset current profile (See the bottom part of Fig. 2).

The injectors differ mainly in the number of holes, orifice shape, and the rail pressure each can achieve. The Spray G orifice diameter is obtained from the ECN information [33]; meanwhile, the diameter in the C3539 case was directly measured by the mean of an electronic microscope.

The testing points were chosen to emulate the conditions found in a real engine, ranging from cold start conditions, early injection, and normal functioning. Specifically, these conditions were selected considering the guidelines proposed by the ECN for the Spray G. In the C3539 case, the energizing time was chosen to set the same hydraulic time found in the Spray G, which makes it easier to compare the results. The main conditions used are summarized in Table 2, even though more particular conditions were measured, especially for the iso-octane fuel, which is the one used as reference.

2.2. Fuels description

The fuels implemented consist of four gasoline surrogates, the ethanol, and a blend made with the latter. The surrogates are iso-octane, n-pentane, n-hexane, and E00. See Table 3.

The main differences between the surrogates implemented are the number of carbon atoms in its chain and, in consequence, some influential properties like the boiling point and the viscosity; all of these variables that affect the spray shape of the sprays [17]. Iso-octane is the component of gasoline with the highest boiling point studied in the present work; the lowest is for n-pentane.

2.3. Mass flow rate instrumentation

Mass flow rate measurements were carried out through an Injection Discharge Rate Curve Indicator (IRDCI) from IAV. This device employs the long tube method to obtain the rate of injection, which has been widely described in the literature [28,37]. The schematic of the devices used to set the conditions pursued and the configuration for the ROI measurements can be appreciated in Fig. 1. The measurement process is described following the fuel path as follows: the fuel is first sucked out from the deposit by the high-pressure system, mainly compounded by a common rail pump, a lubricating pump, and a heat exchanger. The fuel is then delivered at the desired pressure to the common rail (12.3 cm^3) connected to the injector. The injector is fixed to the IDRCI through a jacket holder part designed with accesses through which a continuous coolant flow passes to maintain the nozzle at the desired temperature. Once the injector is electronically actuated, the spray goes to the vessel, and pressure waves are generated. The theory of wave propagation in a liquid column [38,39] allows then calculating the mass flow rate. At the exit of the instrument, the fuel is collected in a gravimetric scale for measuring the mass as a moving average accounting for the number of injections in a period of 100 s. Nitrogen was used to pressurize the IDRCI.

Once the mass collected in the gravimetric scale is stable for the condition, the signal measured by the sensors in the IDRCI is recorded in a digital oscilloscope for a total of 50 injections at ten injections per second rate. The processing of this signal is based on a methodology used in several works [37,40]. As a result, the mass injected is calculated as the integral of the signal and compared to the mass value gathered in the downstream scale. The signal integrated and the mass directly measured usually differ since this method relies upon the values of the speed of sound in the fluid in which the spray is injected, and this value is not quite reported for all fuels used. Additionally, some cycle-to-cycle and temperature variations are present in the process; therefore, a scaling factor is calculated by dividing the mass measured by the integrated one to correct the averaged mass flow rate signal, so both masses (measured and derived) are equal.

2.4. Momentum flux measurement

The rate of momentum measurement consists of the direct measuring of the electrical signal generated in a piezoelectric sensor by the impact of the spray with a flat surface (named target) placed in the sensor and orthogonal to the spray surface. This electrical signal is processed as the force in the axis of the sensor, and based on the conservation of momentum, this force is equal to the momentum flux [28,29]. This method has usually been used in Diesel injectors where the sprays are usually considerably separated (or one-hole injectors), and each jet can be isolated. Nevertheless, in GDI injectors, the situation is different; the sprays are usually closer, and a higher spray to spray interaction is found. Payri et al. [40] analyzed two configurations of the force method with an 8-hole injector, having an increased influence of other sprays in the measurement of an individual one; thus, they concluded that the most accurate method in these injectors is using a frontal configuration with all the jets impacting the target. On the other hand, Cavicchi et al. [29,41] used a lateral configuration measuring the impact of only one spray. The nozzles in their work had equal or less than three holes separated between them, making it possible to capture the sprays separately.

The methodology followed in the present work is a frontal configuration for the global momentum, and the sensor target used has 10 mm of diameter. The basis and equations supporting this technique are widely described in the literature [40–42], and here, only the most important equations will be brought up.

2.4.1. Mass flow rate and momentum relationship

The simplified equations of the definition of the mass flow rate Eq. (1) and momentum Eq. (2) show a close relationship between them.

$$\dot{m} = A\rho_f u \tag{1}$$

$$\dot{M} = A\rho_f u^2 \tag{2}$$

In these equations, $\dot{m}$ is the ROI, A is the exit area of the orifices, ρ_f is the density of the fuel, u is the velocity at the exit, and $\dot{M}$ is the momentum flux or rate of momentum. The velocity is calculated through the Bernoulli equation given by the pressure difference Eq. (3).

$$uth = \sqrt{2 * \Delta P/\rho_f} \tag{3}$$

If cavitation takes place in the nozzle, the flow through the outlet area is not homogeneous and is likely not to use the total exit area; thus, an effective area and velocity can be defined as the actual area or velocity over the nominal area or theoretical velocity. The same principle is used to define non-dimensional coefficients to characterize the injectors at different conditions, such as the discharge coefficient (C_d) and velocity coefficient (C_v) that are the most commonly employed (Eqs. (4) and (5)). The other parameters are calculated from equations reported in other works [37,40,42].

$$C_d = \frac{\dot{m}}{A\rho_f u} \tag{4}$$

Table 2
Test plan for the measurements and ECN conditions.

Parameter	Operating value	Units	ECN standard	G2 flash boiling	G3 early injection	G4 Strong collapse
Rail pressure (P_r)	100–200–350[b]	bar	200	200	200	200
Ambient pressure (P_b)	0.2[a]–0.5[a]–1[a]–2–6–15–21.5	bar	6	0.5	1	21.5
Injector operating temperature	20–90	°C	90	90	90	90
Ambient temperature	25	°C	300	60	60	300
Energizing time	680–810[b]	µs	680	680	680	680
Hydraulic time	780	µs	780	780	780	780
Injection frequency	2[a]–10	Hz	–	–	–	–
Injection cycles	50	–	–	–	–	–

[a]Only for rate of momentum campaign.
[b]Only for the C3539 injector [34].

Table 3
Fuel properties.

Fuel	Chemical formula/Blend	Density [kg m^{-3}]	Viscosity [mPa s]	Boiling point [°C][a]
Iso-octane	C_8H_{18}	690.3	0.47	99.26
Hexane	C_6H_{14}	654.78	0.22775	68.71
Pentane	C_5H_{12}	621.7	0.29628	36.06
Ethanol	C_2H_6O	789.1	1.074	78.35
E00	46% iso-octane			
	36% n-pentane,	711.76	0.2465	
	18% n-undecane,			
E20	80% E00, 20% ethanol,	725		

[a]At ambient temperature.
For properties source [34–36].

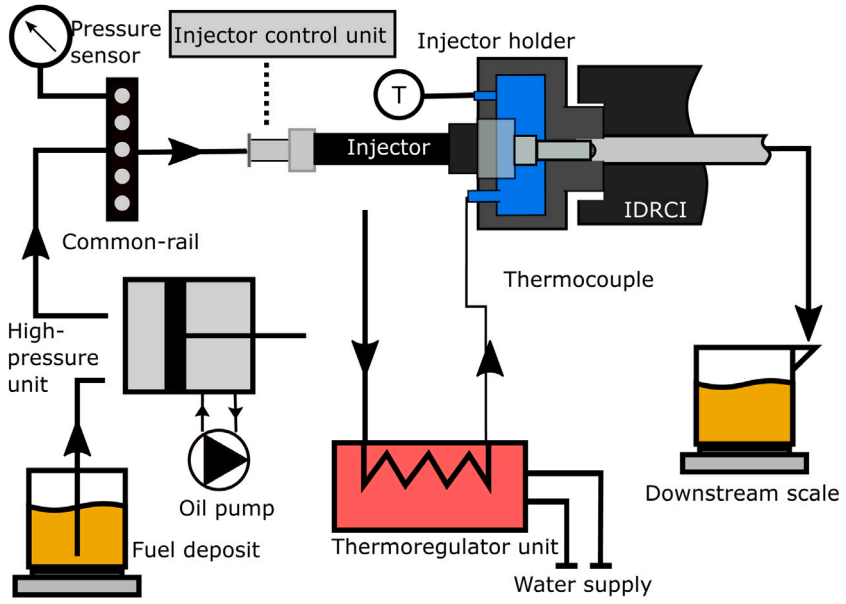

Fig. 1. Schematic diagram of the mass flow rate measurement.

$$C_v = \frac{u_{ef}}{u_{th}} \tag{5}$$

Finally, the area coefficient (C_a) can be calculated from the (C_d) and (C_v), Eq. (6).

$$C_a = \frac{C_d}{C_v} \tag{6}$$

2.4.2. Measurement of spray core angle

The ROM characterization requires knowing the angle of inclination of the sprays with respect to the injector axis. It is necessary to ensure that all sprays are impacting the target in the sensor (one of the method's assumptions). To this aim, an adaptation of the plastic deformation technique used by Shahangian et al. [43] is carried out. Here, the fuel is injected onto a millimetric paper placed over a flat surface in front of the nozzle tip. Several injections are done until the sprays penetrate the paper. Later, moving the paper's position in the axial direction, at known separations between it and the nozzle tip, the coordinates of the points can be mapped along the axis so that by trigonometry and an internally developed code, the approximate angle of the spray cores can be calculated.

On the other side, the angles calculated are used to correct the momentum signal, which Shahangian et al. [43] did by means of Eq. (7). The sprays for both injectors are symmetrical to the injector axis.

$$M_c = \sum_{i=1}^{n} \frac{M_m/n}{\cos\alpha_i} \tag{7}$$

Where M_m is the total momentum measured, n is the number of orifices that are impacting the sensor and α_i is the angle of each core jet with respect to the sensor surface.

3. Results and discussion

In this section the mass flow rate results are presented, comparing how each injection variable affects the injected mass and the curve itself, later, a comparison between the tested fuels and both injectors are going to be contrasted. Later, the same comparisons for momentum flux results can be found and finally the flow coefficients. Although many conditions were tested, only the main conditions are going to be shown proving the main findings of the work.

3.1. Mass flow rate signal

The global ROI of 50 cycles obtained for an injection pressure of 200 bar and an ambient pressure of 6 bar are shown in Fig. 2 for the Spray G on the left and C3539 on the right. The 50 cycles are filtered by a shot-to-shot deviation analysis through the residuals and the sigma values of a fit robust linear regression. The repetitions are then averaged so the comparison among conditions can be done. The most important parts of the curve to be analyzed are the beginning of it which corresponds to the needle opening of the injector, and the stabilized part of the curve which is the representative of the steady state operation at each condition. At the end of the injection some oscillations can be appreciated, which are presumably a result inherent to the mass flow rate technique. The waves generated by the injection travel through the long tube and can generate those curves. The limits of the stable part used to calculate the mass flow is marked with vertical lines in the plot. In overall, the limits were chosen in the 45% to 50% of the injection duration. Overall, the limits were chosen to cover 45% to 50% of the injection duration, from 20% to 70% of the total injection time. The start and end of injection is calculated with a linear fit of the rising and falling edge of the signal. The rising edge is found in the first points between 10% and 20% of the maximum mass flow rate measured. The falling edge follows the same analogy between 35% and 50% of the maximum value got for the y-axis. The start of injection is later adjusted with the sound velocity and the distance to the sensor to account for the delays induced by this distance. Good agreement is seen between the repetitions, with a low shot to shot dispersion ranged from 1% to 3%.

The electrical signal to activate the injectors is provided by its particular ECU and it is depicted in the bottom of Fig. 2. The pressure drop is also recorded to corroborate the variation in the pressure. In the C3539 injector the pressure is more stable for the same injection pressure, although, for higher pressures the drop was more pronounced. The more stable signal in the C3539 can be explained by the bigger volume in the fuel inlet.

3.1.1. Vessel pressure and nozzle temperature effect

Figs. 3 and 4 show the back pressure effect in the mass flow rate. As it has been reported in the literature for GDI, the mass flow rate does not change significantly with the back pressure since the difference between injection pressure and back pressure is low [40]; however, for the C3539, for high ambient pressures, the fuels which do not contain ethanol showed a slightly higher steady ROI (Fig. 4); nevertheless, the differences are negligible and can be attributed to differences in measurement. On the other hand, the opening presents some changes in the overshot that is more pronounced for lower back pressure, and as it increases, the opening overshot is smoother. This behavior was only different for the Spray G with ethanol and the E20. With the addition of ethanol, the overshot is quite smooth, and for the ethanol, it disappears for all back pressures tested. The ethanol and E20 were not measured at the 21.5 bar counterpressure.

The influence of the nozzle temperatures for each injector is also analyzed since it is a parameter that influences the spray shape and affects processes as flash boiling or spray collapse [44]. Fig. 5 shows the temperature effect that can be visualized in variations of two parts of the ROI lines. Elevating the temperature results in the stable mass flow rate increasing towards the second half of the injection, and for the C3539 injector, the injection duration also increases. For the ethanol, the start of injection (SOI) is advanced for the higher temperature; however, this is not seen for other fuels. The SOI is defined by the hydraulic delay, which is the difference between the moment the electric signal is sent to the injector and when the actual injection starts. This delay is affected by several factors like the fuel viscosity, the needle lift, the nozzle type, among others. For the case in Fig. 5, the shorter SOI might be because of the changes in the viscosity [38,45]. For lower viscosity, the needle movement is faster, then allowing the fuel to come out quicker. The effect is more evident for the ethanol, presumably due to the magnitude of each fuel viscosity variation depending on the temperature. For the hexane, for instance, the viscosity decreases around 43% when increasing the temperature, but, for ethanol, the diminution is 69% [36].

3.1.2. Fuel comparison

Fig. 6 shows the difference between the rate of injection between the different fuels for 6 bar of back pressure and 200 bar of injection pressure. The subplots are divided by injectors column-wise and for nozzle temperature row-wise. Several aspects can be evaluated from this Figure. First, the ethanol curve outstands over the others, the curve is displaced to the right in the time axis, meaning that the SOI is delayed for this fuel. The same effect was observed for other injection and back pressures, although greater for higher injection pressures. On the other side, the hexane shows a slightly shorter SOI, especially at low injection pressure and temperature, and the same stable ROI as the E00 and E20 blends. In the case of isooctane, it is close in the ROI to the Ethanol for the C3539 injector.

This different behavior seen for the ethanol might be due to the fuel properties. To start with, the ethanol is the most viscous and densest fuel tested. The higher viscosity slows down the needle movement and makes it difficult to reach a complete opening [38,46]. This can be observed both in the retarded SOI and in the initial curve slope, which is smoother for the ethanol and more noticeable at ambient temperature. In this regard, as seen in the previous section, at 90 °C the viscosity decreases and the SOI is closer to the other fuels. Referring to the higher ROI encountered for the ethanol, this might be due to its density. Payri et al. [47] also found that for two fuels analyzed; the denser had a higher ROI. On the other side, adding 20% of ethanol to the E00 blend did not induce any change in the ROI.

It is important to comment that the ethanol had almost the same ROI as the other fuels, especially the Isooctane for lower injection pressure. This suggests that the effect of the fuel density is not determinant at low injection pressure. Fig. 7 condenses the information of the main variables measured for the rate of injection for both injectors and all fuels. Two groups are seen, one for higher injection pressure and one for the lower. Slight differences are seen in the ROI for the surrogates, except for the Isooctane, which follows the ethanol at the highest ROI. Meanwhile, the differences in the other are not significant.

3.1.3. Injector comparison

Fig. 8 displays the ROI for both injectors in different line styles. The injection pressure is represented by different colors. The left subplot is for the total mass flow rate injected, and the right is the result of dividing the total ROI by the number of orifices of each injector.

One aspect to mention is that the global ROI of the Spray G at 200 bar has about the same mass flow rate as the C3539 injector at 350 bar, which is important due to the numerous benefits that higher injection pressures provide in the spray development and atomization process, that for this injector can be achieved by maintaining the same injected quantity as the Spray G, which matches the design target of last generation GDI injectors of achieving a given flow rate level with small holes to obtain lower PM emission.

A fairer comparison between injectors is made to the right of Fig. 8 when the ROI per orifice is contrasted. The individual holes of the

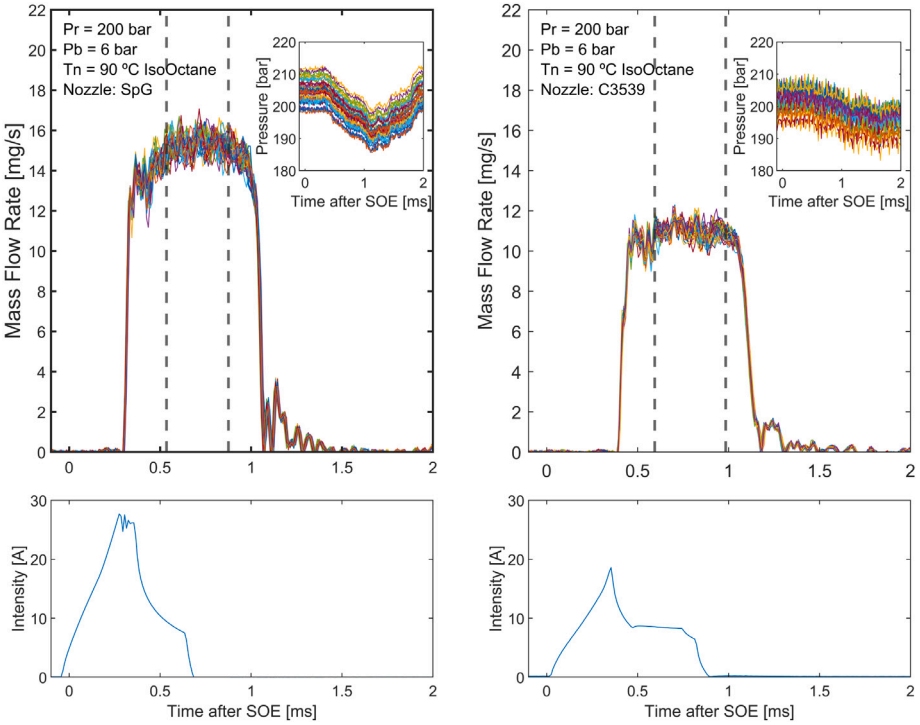

Fig. 2. Rate of Injection of the Spray G (left) and C3539 (right) for ECN standard condition: Pr = 200 bar, Pb = 6 bar and nozzle temperature of 90°. At the top right the pressure plot can be observed and in the bottom the electrical signal for the activation.

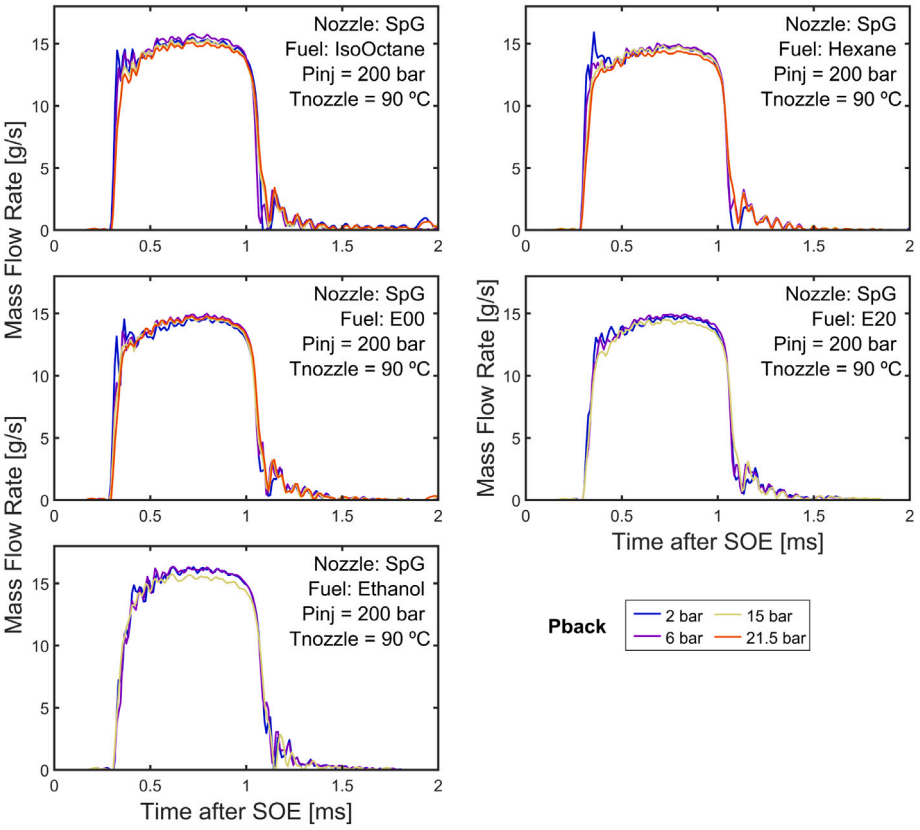

Fig. 3. Effect of the back pressure in the Rate of injection for different fuels for the Spray G injector.

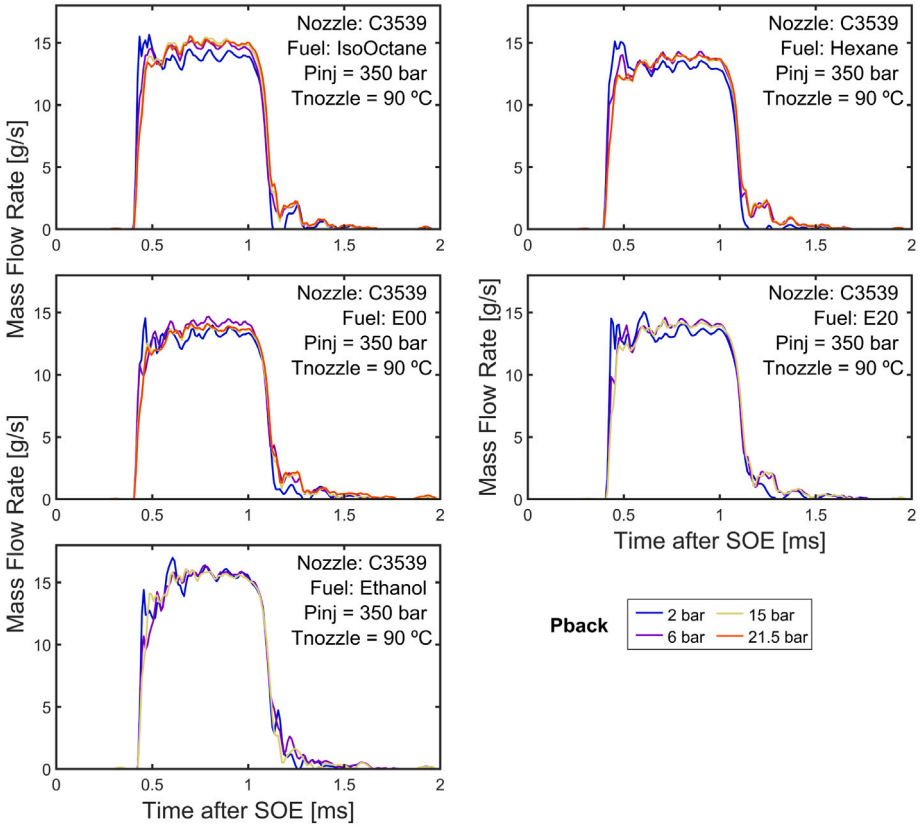

Fig. 4. Effect of the back pressure in the Rate of injection for different fuels and conditions for the C3539 nozzle.

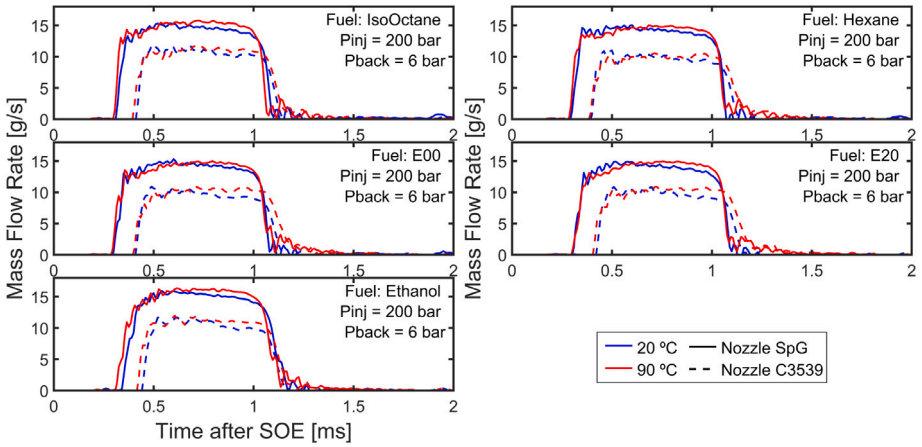

Fig. 5. Nozzle Temperature effect in the rate of injection for different fuels.

injectors depict the same ROI; thus, the differences in the global result are determined by the number of orifices that each has and the injection pressure they are capable of reaching. Besides, due to the smaller C3539 hole diameter and the cylindrical orifice type, higher discharge coefficients are expected.

In the Figure, the difference between the start of energizing and the start of injection is shorter for the C3539 injector. The difference is probably due to the each injector design. Other external influences from the measurement, such as the differences in the distance of the position of each injector, are discarded. The injector's holders aim to have both injector's tips at the same position and the same distance to the wave sensor in the vessel. Therefore, for discrepancies of ± 2 mm in the positioning of the injectors, the time difference in the hydraulic delay would be around 6.4 μs (using the Bernoulli equation with higher ΔP) which is negligible against the difference for the SOI about 110 μs between injectors.

The rail pressure effect on the ROI can also be commented on from this figure. From the theoretical background, it is well known that the injection pressure increases the velocity, and thence, the ROI magnitude. In the transient opening and closing, for both injectors, the curve behaves the same; however, important differences are found during closing transients for the Spray G injector. As the injection pressure increases, the injection duration decreases for the same energizing time, which represents an essential factor to take into account for the total injected mass since it is not enough to know the stable mass flow rate. Still, the duration as a function of the injection pressure also needs to be considered. This behavior can be explained by higher fuel pressures increasing the needle closing velocity as found by Cavicchi and Postrioti

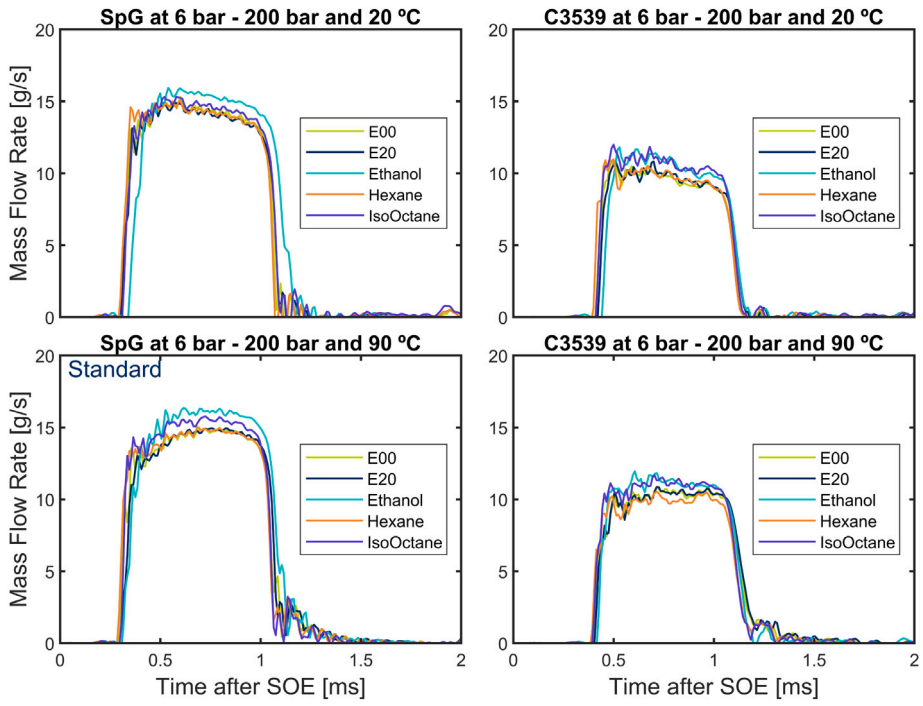

Fig. 6. Effect of the fuel in the Rate of injection for various conditions including the ECN standard condition.

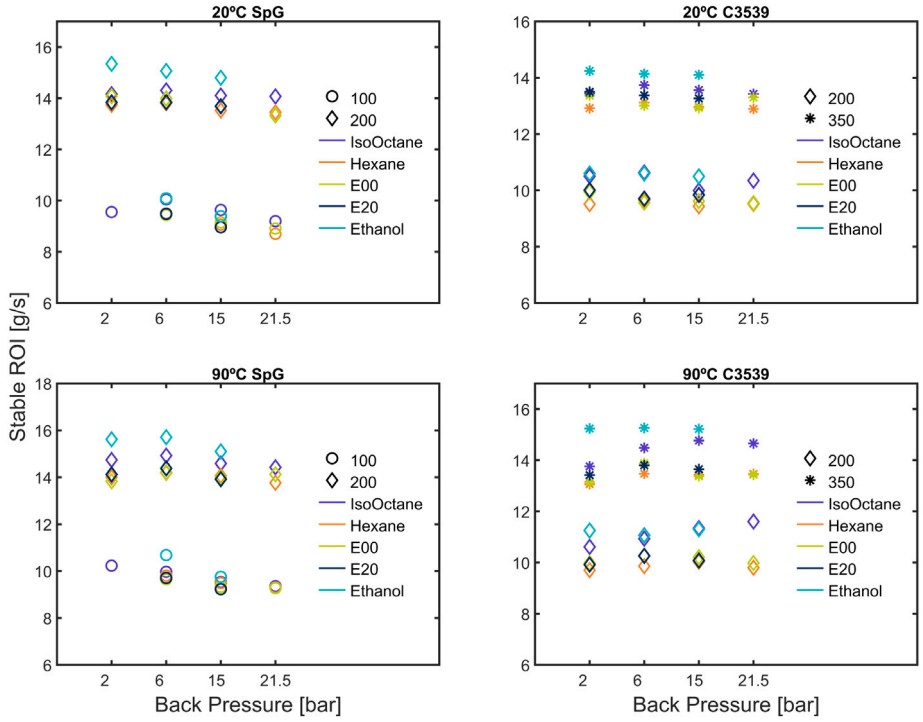

Fig. 7. Effect of the back pressure in the stabilized Rate of injection for different fuels and conditions.

[48]; however, this is not found in the C3539 injector; thus, the injector design, the string force, and needle motion of each injector also have an effect on this trend.

3.2. Momentum flux results

As it was mentioned in Section 2.4.2, the distance between the sensor and the nozzle tip must be considered in the momentum flux measurement for setting the distance between the sensor and the injector. Hence, the target captures the entire spray. To this aim, the described methodology for the sprays' core angle (Section 2.4.2), together with the results obtained for the visualization of the Spray G jets made by Bautista Rodríguez [49] for the Spray G nozzle who showed a description of the spray width along the nozzle axis allowed to set a limit to the distance at which the sensor could be placed while being confident that the impingement area of the spray is smaller than that of the sensor target.

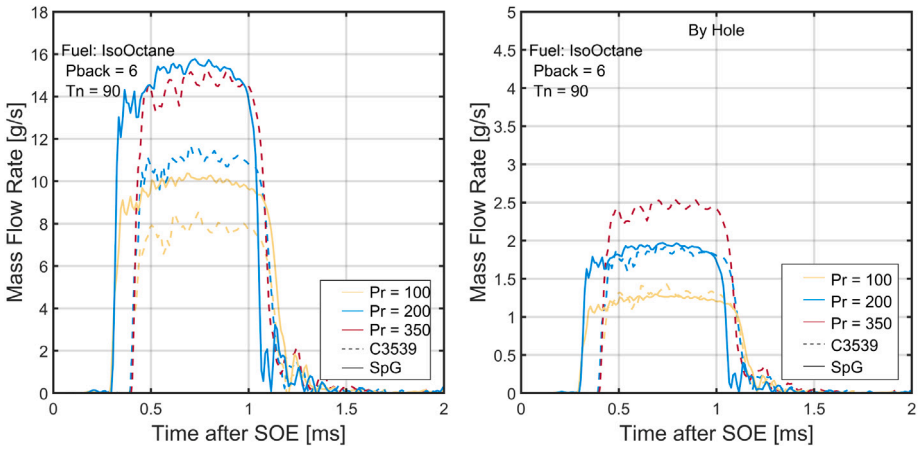

Fig. 8. Rate of injection for both injectors and different inejection pressures. To the right the global rate of injection is showed, to the right it is shown divided by the injector number of orifices.

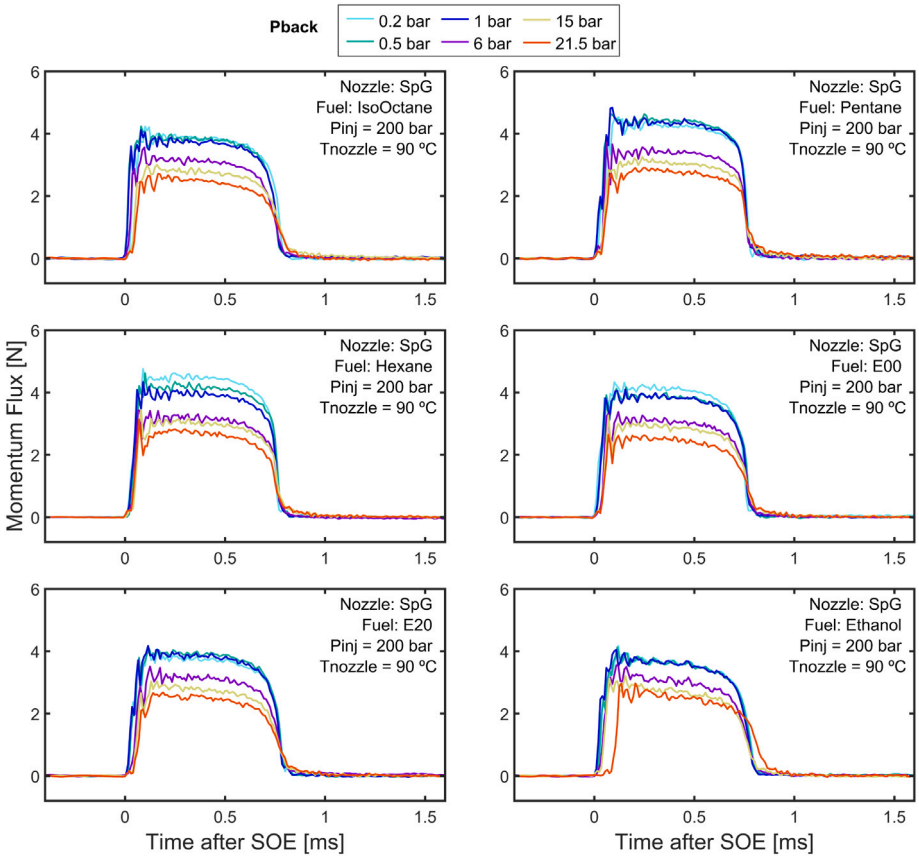

Fig. 9. Effect of the back pressure in the Rate of momentum for different fuels in the Spray G injector.

This principle was verified through a separation analysis. The momentum keeping one operating condition was measured for distances from 0.5 mm to 5 mm between the sensor target and the nozzle tip. The values remain the same as long as the spray is fully captured; thence, when the target is too far, parts of the spray are lost, and consequently, the momentum decreases. For the spray G injector, the distance selected was 2.1 mm, and for the C3539, 2.4 mm.

3.2.1. *Vessel pressure effect*

Figs. 9 and 10 show the results obtained for the different back pressures for injection pressures of 200 bar in the case of Spray G nozzle and 350 bar for the C3539 injector.

For the discharge pressures studied, the ROM at 6, 15 and 21.5 bar are very similar to the trend seen in the Shahangian et al. [43] results, in which some variations in the ROM due to the back pressure were found. The authors attributed these differences to the change in density in the discharge ambient. Payri et al. [40] tested the momentum for two ambient gas and encountered that, indeed, the ambient density has an effect on the result for this configuration. Something that is not found when studying an isolated spray jet. These discrepancies are not considered decisive in these previous studies; nevertheless, conditions with values equal or under atmospheric pressure in the present investigation are together separated from the other lines. This behavior suggests that due to the low gas density at 0.2, 0.5 or 1 bar. These

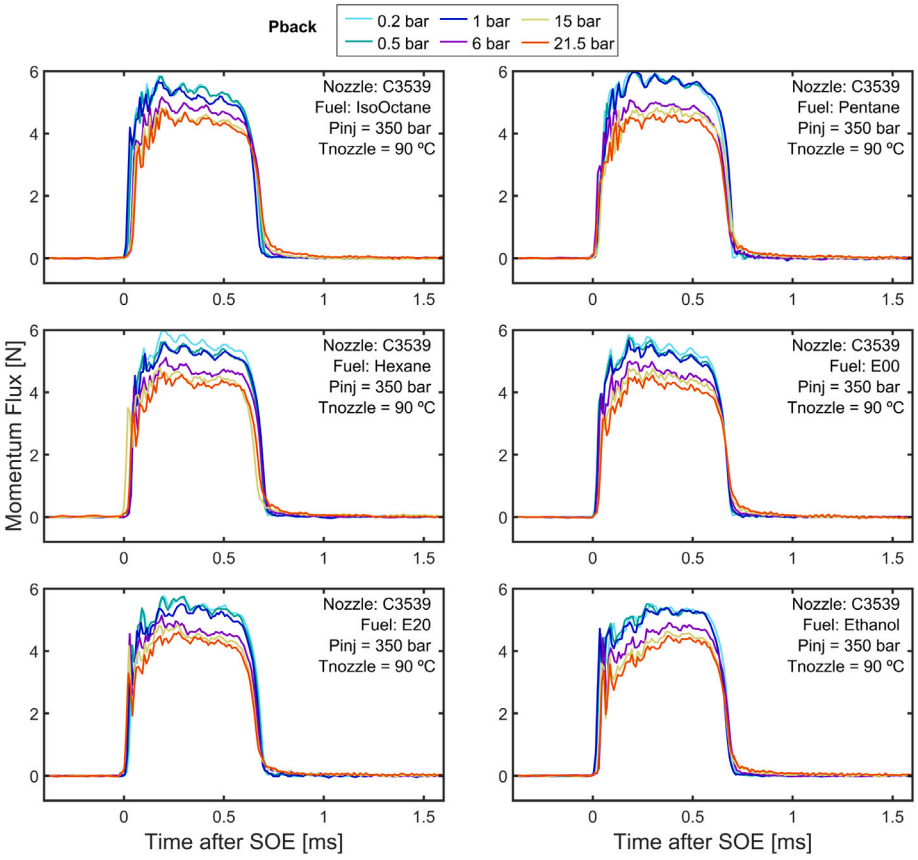

Fig. 10. Effect of the back pressure in the Rate of Momentum for different fuels for the C3539 injector.

trends are expected from the theoretical analysis made for momentum; although, these variations could also be influenced by the spray angle variation impacting the target surface.

Considering that the global momentum measured has to be corrected with the cone angles, the changes in the latter affect the results. Bautista Rodríguez [49] reported that with flash boiling and spray collapse conditions, which is the case of sub-atmospheric pressures at nozzle temperature of 90 °C for all fuels studied in this work, the angle of the injector changes significantly; therefore, the angle input in the correction factor (Eq. (7)) also varies, affecting the correction process. Although, it can be brought up that the variation is not high in the first 5 mm. However, the difficulties in accurately determining the angle make it difficult to correlate with the momentum correction directly.

3.2.2. Fuel and injector comparison

Fig. 11 contains the information about the influence of the fuel on the momentum flux. No important variations are found, only at low ambient nozzle temperature, the SOI for the ethanol is retarded with respect to the other fuels in the case of the C3539 injector; equally, the overshot in the opening is higher at this temperature. The reasons for these changes in the SOI of the ethanol are related to the higher viscosity of the fuel. This is already explained in Section 3.1.2 in which the differences are clearer since coinciding the theoretical equations (Eq. (2) combined with Eq. (3)) in which the momentum is only dependent on the area and pressure drop. This was also confirmed by Payri et al. [47], who demonstrated that the injection rate in mass is affected by fuel density, but the spray momentum is not.

Fig. 12 reports the differences found for both injectors. The plots are phased with respect to the SOI. The plot to the right represents the ROM of each orifice, assuming they all contribute the same to the global force. The ROM per hole is the same for both injectors, even though the diameter of the holes of the Spray G injector is bigger than the C3539 ones. That equality also matches with the literature in which it is stated that the ROM depends on the pressure difference and fuel properties. Thus, the differences in the global force are due to the number of holes.

Having the same momentum for different hole diameters indicates that the injector with smaller orifices has an exit velocity closer to that theoretical, and higher hydraulic coefficients are expected. This claim can be corroborated by the calculation of them that are described in the next Section 3.3.

3.3. Hydraulic coefficients

Having both ROI and ROM results, the flow coefficients can be calculated as explained in Section 2.4.1 with the equations obtained from the literature [28,37,41]. The coefficients were only calculated for the conditions realized for both ROI and ROM. In Fig. 13, results of the discharge coefficients at 200 bar of injection pressure are shown on the left, and the coefficient of velocity on the right.

The trends match those reported in other works [40] for the Spray G. The magnitude of the discharge coefficient does not vary much for the Spray G with the changes in the pressure drop. However, a different tendency is seen for the C3539, especially at higher nozzle temperatures; in which the C_d has an inverse correlation with respect to the square root of the pressure drop rise; as it was observed either when increasing the injection pressure or when decreasing the counter pressure, that the C_d falls substantially. This trend was observed only for iso-octane and, to a lesser extent, hexane. The magnitude of the discharge coefficient does not present marked discrepancies between the fuels.

The C3539 injector has markedly more discharge coefficient values than the Spray G, which indicates that the hole's area used by this injector is closer to the geometrical one, as it was commented for the ROM results. The velocity coefficient (C_v) was higher for higher

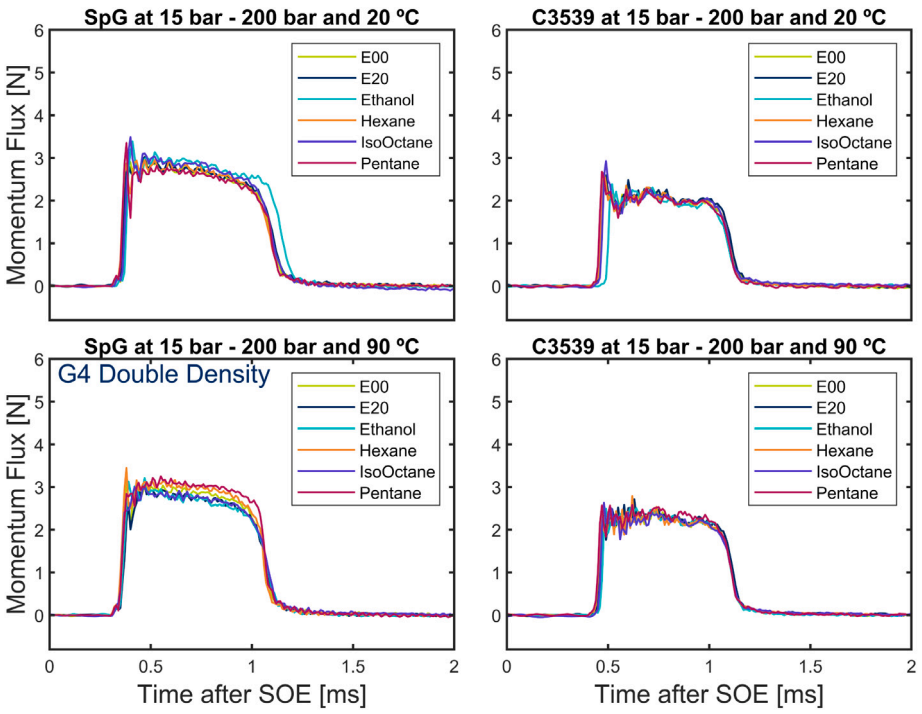

Fig. 11. Effect of the fuel in the rate of momentum for various conditions including the ECN double density.

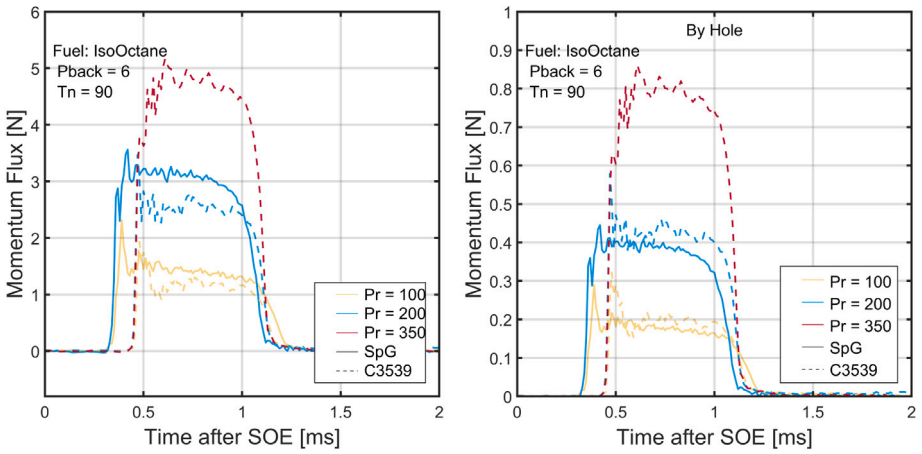

Fig. 12. Rate of momentum for both injectors and different injection pressures. On the left the global rate of injection is showed, to the right it is shown divided by the injector number of orifices.

pressure drops for both injectors. Regarding the differences in the C_v between injectors, the C3539 nozzle also presented higher values.

4. Conclusions

Investigations on the different parameters that have a remarkable influence on the rate of injection (ROI) and rate of momentum (ROM) have been realized. Several back pressures and injection pressures were studied for two nozzle temperatures, five fuels (six for the momentum flux), and two GDI injectors. The fuels studied are three paraffin, which are mono components of the commercial gasoline, two blends, and one alcohol (Ethanol). The injection variables were chosen aiming at the conditions found in the normal functioning of an engine and mainly following the conditions suggested by the ECN for cold start, early injection, and strong collapse, conditions that have not been extensively experimented for this type of injectors and fuels. The main findings are described as follow:

- The ROI did not have a significant change for the surrogates. It was only slightly different for the ethanol. The effects of this fuel are presumed to be because of its higher density and viscosity. In agreement with the literature, denser fuels are likely to increase the ROI, with the viscosity changing the transient opening and closing of the injector, not only in its needle lift velocity but also in the delay of the start of injection.
- For the injection pressure and nozzle temperature, the same behavior reported in the literature is found. As the injector pressure increased, the ROI and ROM rose as well. Augmenting the temperature increased the injection duration due to the reduction of the fuel viscosity.
- The injectors studied depict the exact ROI and ROM per orifice, although having different hole diameter and nozzle geometry. Due to the higher number of holes, the Spray G injector can reach a higher ROI for the same injection pressure. However, the C3539 can get higher injection pressures, providing some advantages in

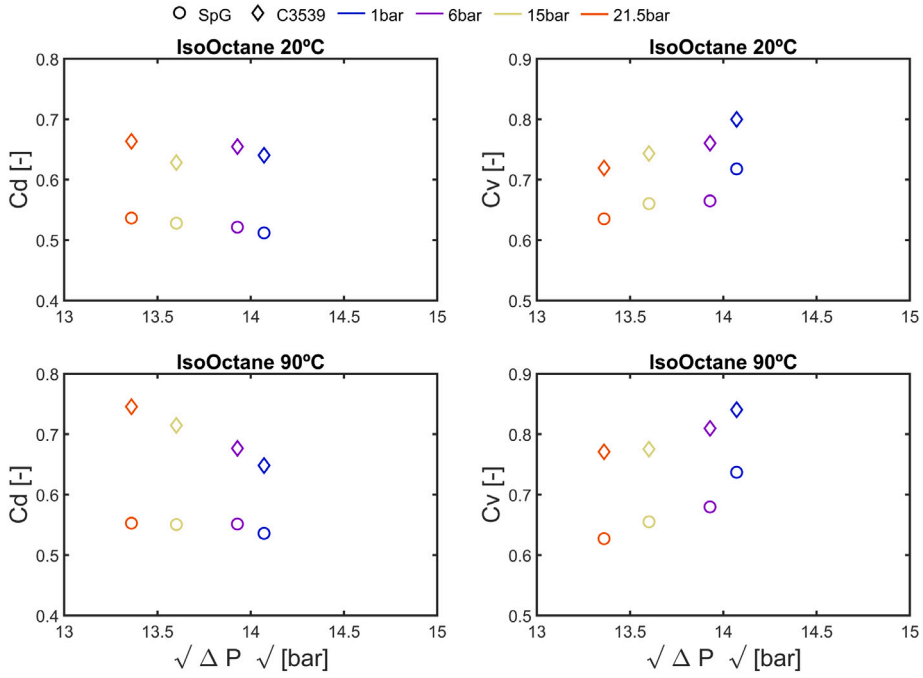

Fig. 13. Discharge Coefficient and Velocity coefficient vs the square root of the pressure drop. The colors represent the ambient pressure and the symbols are distinctive of each injector. (For interpretation of the references to color in this figure legend, the reader is referred to the web version of this article.)

terms of atomization (according to the literature) and giving the chance to have more controllability.
- The ROM did not suffer significant changes for the fuels. Again, the ethanol induced a delay in the SOI for cold conditions.
- The discharge coefficient (C_d) of the C3539 injector depicted higher values than the Spray G injector. Even though for both injectors, the Cd did not vary much with the pressure drop, for the C3539 injector, the Cd decreased for higher ΔP.

CRediT authorship contribution statement

Raul Payri: Supervision, Funding acquisition. **Jaime Gimeno:** Methodology, Validation. **Pedro Marti-Aldaravi:** Data curation, Writing – review & editing. **Victor Mendoza Alvarez:** Investigation, Writing – original draft.

Declaration of competing interest

The authors declare that they have no known competing financial interests or personal relationships that could have appeared to influence the work reported in this paper.

Acknowledgments

This work has been partially funded by Generalitat Valenciana "Nuevos conceptos en inyección de gasolina (NCIG)", Spain with AICO/2020/208 reference. The author Victor Mendoza thanks the Universitat Politècnica de València, Spain for his predoctoral contract, which is included within the framework of "Programa Propio de la Universitat Politècnica de València - Subprograma 1 (PAID-01-20)".

References

[1] Chincholkar S, Suryawanshi J. Gasoline direct injection: an efficient technology. Energy Procedia 2016;90:666–72.

[2] O'Driscoll R, Stettler ME, Molden N, Oxley T, ApSimon HM. Real world CO2 and NOx emissions from 149 Euro 5 and 6 diesel, gasoline and hybrid passenger cars. Sci Total Environ 2018;621:282–90.

[3] Saliba G, Saleh R, Zhao Y, Presto AA, Lambe AT, Frodin B, Sardar S, Maldonado H, Maddox C, May AA, et al. Comparison of gasoline direct-injection (GDI) and port fuel injection (PFI) vehicle emissions: emission certification standards, cold-start, secondary organic aerosol formation potential, and potential climate impacts. Environ Sci Technol 2017;51:6542–52.

[4] Bieker G. A global comparison of the life-cycle greenhouse gas emissions of combustion engine and electric passenger cars. Technical report July, The International Council on Clean Transportation; 2021.

[5] Nour M, Sun Z, Cui M, Yang S, Hung D, Li X, Xu M. Effect of flash boiling injection on combustion and PN emissions of DISI optical engine fueled with butanol isomers/TPRF blends. Proc Combust Inst 2021;38:5923–31. http://dx.doi.org/10.1016/j.proci.2020.10.006.

[6] Leach F, Knorsch T, Laidig C, Wiese W. A review of the requirements for injection systems and the effects of fuel quality on particulate emissions from GDI engines. SAE Tech Pap 2018;2018-Septe. http://dx.doi.org/10.4271/2018-01-1710.

[7] Raza M, Chen L, Leach F, Ding S. A review of particulate number (PN) emissions from gasoline direct injection (GDI) engines and their control techniques. Energies 2018;11. http://dx.doi.org/10.3390/en11061417, URL https://www.mdpi.com/1996-1073/11/6/1417.

[8] Lee Z, Park S. Particulate and gaseous emissions from a direct-injection spark ignition engine fueled with bioethanol and gasoline blends at ultra-high injection pressure. Renew Energy 2020;149:80–90. http://dx.doi.org/10.1016/j.renene.2019.12.050.

[9] Stadler A, Brunner R, Wachtmeister G, Sauerland H. Experimental investigations on high pressure gasoline injection up to 800 bar for different combustion modes. MTZ Worldwide 2019;80:52–7. http://dx.doi.org/10.1007/s38313-018-0161-y.

[10] Liu Y, Pei Y, Peng Z, Qin J, Zhang Y, Ren Y, Zhang M. Spray development and droplet characteristics of high temperature single-hole gasoline spray. Fuel 2017;191:97–105. http://dx.doi.org/10.1016/j.fuel.2016.11.068.

[11] Duan Y, Shi X, Kang Y, Liao Y, Duan L. Effect of hydrous ethanol combined with EGR on performance of GDI engine. Technical report, SAE Technical Paper; 2020.

[12] Gao J, Chen H, Liu Y, Laurikko J, Li Y, Li T, Tu R. Comparison of NOx and PN emissions between Euro 6 petrol and diesel passenger cars under real-world driving conditions. Sci Total Environ 2021;801:149789.

[13] Duronio F, De Vita A, Montanaro A, Villante C. Gasoline direct injection engines – A review of latest technologies and trends. Part 2. Fuel 2020;265:116947. http://dx.doi.org/10.1016/j.fuel.2019.116947.

[14] Sher E, Bar-Kohany T, Rashkovan A. Flash-boiling atomization. Progress Energy Combust Sci 2008;34:417–39. http://dx.doi.org/10.1016/j.pecs.2007.05.001, URL http://linkinghub.elsevier.com/retrieve/pii/S0360128507000500.

[15] Shirazi SA, Abdollahipoor B, Windom B, Reardon KF, Foust TD. Effects of blending C3-C4 alcohols on motor gasoline properties and performance of spark ignition engines: A review. Fuel Process Technol 2020;197:106194. http://dx.doi.org/10.1016/j.fuproc.2019.106194.

[16] Li X, Sun Z, Yang S, Wang H, Nour M. Flash boiling combustion of isomeric butanol and gasoline surrogate blends using constant volume spray chamber and GDI optical engine. Fuel 2021;286:119328. http://dx.doi.org/10.1016/j.fuel.2020.119328.

[17] Aleiferis PG, Van Romunde ZR. An analysis of spray development with iso-octane, n-pentane, gasoline, ethanol and n-butanol from a multi-hole injector under hot fuel conditions. Fuel 2013;105:143–68. http://dx.doi.org/10.1016/j.fuel.2012.07.044.

[18] Duronio F, De Vita A, Allocca L, Anatone M. Gasoline direct injection engines – A review of latest technologies and trends. Part 1: Spray breakup process. Fuel 2020;265:116948. http://dx.doi.org/10.1016/j.fuel.2019.116948.

[19] Lacey J, Kameshwaran K, Sathasivam S, Filipi Z, Cannella W, Fuentes-Afflick PA. Effects of refinery stream gasoline property variation on the auto-ignition quality of a fuel and homogeneous charge compression ignition combustion. Int J Engine Res 2017;18:226–39.

[20] Piehl JA, Zyada A, Bravo L, Samimi-Abianeh O. Review of oxidation of gasoline surrogates and its components. J Combust 2018;2018. http://dx.doi.org/10.1155/2018/8406754.

[21] Kraus F, Martins Oliveira AA, Bueno Bontorin AC, Rouge dos Santos A, Cancino LR. I-pentane and i-pentene as gasoline surrogates for the transport industry: a numerical analysis on ignition delay times using detailed chemical kinetics. In: Brazilian congress of thermal sciences and engineering. 2020, http://dx.doi.org/10.26678/abcm.encit2020.cit20-0512.

[22] da Costa RBR, Valle RM, Hernández JJ, Malaquias ACT, Coronado CJ, Pujatti FJP. Experimental investigation on the potential of biogas/ethanol dual-fuel spark-ignition engine for power generation: Combustion, performance and pollutant emission analysis. Appl Energy 2020;261:114438. http://dx.doi.org/10.1016/j.apenergy.2019.114438.

[23] Fan Q, Liu S, Qi Y, Cai K, Wang Z. Investigation into ethanol effects on combustion and particle number emissions in a spark-ignition to compression-ignition (SICI) engine. Energy 2021;233:121170. http://dx.doi.org/10.1016/j.energy.2021.121170.

[24] McCaffery C, Durbin TD, Johnson KC, Karavalakis G. The effect of ethanol and iso-butanol blends on polycyclic aromatic hydrocarbon (PAH) emissions from PFI and GDI vehicles. Atmosph Pollut Res 2020;11:2056–67. http://dx.doi.org/10.1016/j.apr.2020.08.024.

[25] Gao J, Jiang D, Huang Z. Spray properties of alternative fuels: A comparative analysis of ethanol-gasoline blends and gasoline. Fuel 2007;86:1645–50. http://dx.doi.org/10.1016/j.fuel.2006.11.013.

[26] El-Faroug MO, Yan F, Luo M, Fiifi Turkson R. Spark ignition engine combustion, performance and emission products from hydrous ethanol and its blends with gasoline. Energies 2016;9. http://dx.doi.org/10.3390/en9120984, URL https://www.mdpi.com/1996-1073/9/12/984.

[27] Turner D, Xu H, Cracknell RF, Natarajan V, Chen X. Combustion performance of bio-ethanol at various blend ratios in a gasoline direct injection engine. Fuel 2011;90:1999–2006. http://dx.doi.org/10.1016/j.fuel.2010.12.025.

[28] Gimeno J. Desarrollo y aplicación de la medida de flujo de cantidad de movimiento de un chorro Diesel. [Ph.D. thesis], E.T.S. Ingenieros Industriales, Universidad Politécnica de Valencia; 2008, http://dx.doi.org/10.4995/Thesis/10251/8306, URL https://riunet.upv.es/handle/10251/8306.

[29] Cavicchi A, Postrioti L, Giovannoni N, Fontanesi S, Bonandrini G, Di Gioia R. Numerical and experimental analysis of the spray momentum flux measuring on a GDI injector. Fuel 2017;206:614–27. http://dx.doi.org/10.1016/j.fuel.2017.06.054, URL http://linkinghub.elsevier.com/retrieve/pii/S0016236117307627.

[30] Mohapatra CK, Schmidt DP, Sforozo BA, Matusik KE, Yue Z, Powell CF, Som S, Mohan B, Im HG, Badra J, Bode M, Pitsch H, Papoulias D, Neroorkar K, Muzaferija S, Martí-Aldaraví P, Martínez M. Collaborative investigation of the internal flow and near-nozzle flow of an eight-hole gasoline injector (Engine Combustion Network Spray G). Int J Engine Res 2020. http://dx.doi.org/10.1177/1468087420918449.

[31] Shahangian N, Sharifian L, Uehara K, Noguchi Y, a Martí nez M, Aldaraví PM, Payri R. Transient nozzle flow simulations of gasoline direct fuel injectors. Appl Therm Eng 2020;175:115356. http://dx.doi.org/10.1016/j.applthermaleng.2020.115356, URL https://www.sciencedirect.com/science/article/pii/S1359431120301745.

[32] Di Ilio G, Krastev VK, Falcucci G. Evaluation of a scale-resolving methodology for the multidimensional simulation of GDI sprays. Energies 2019;12. http://dx.doi.org/10.3390/en12142699, URL https://www.mdpi.com/1996-1073/12/14/2699.

[33] Engine Combustion Network. 2010, https://ecn.sandia.gov/diesel-spray-combustion/.

[34] Engine Combustion Network. Spray G parametric variation. 2020, Accessedon29April2020.

[35] Lemmon EW, Bell I, Huber M, McLinden MO. Thermophysical properties of fluid systems. In: Linstrom PJ, Mallard WG, editors. NIST Standard Reference Database Number 69. Gaithersburg MD, 20899, USA.: National Institute of Standards and Technology; 1998, http://dx.doi.org/10.18434/T4D303.

[36] Pérez-Ones O, Díaz-Rodríguez J, Zumalacárregui L, Gozá-León O. Evaluación de propiedades físicas de mezclas etanol-agua (II). Revista Facultad De IngenieríA Universidad De Antioquia 2010;62–74.

[37] Payri R, Gimeno J, Martı Aldaravi P, Viera A. Measurements of the mass allocation for multiple injection strategies using the rate of injection and momentum flux signals. Int J Engine Res 2020. http://dx.doi.org/10.1177/1468087419894854.

[38] Salvador FJ, Gimeno J, Carreres M, Crialesi-Esposito M. Fuel temperature influence on the performance of a last generation common-rail diesel ballistic injector. Part I: Experimental mass flow rate measurements and discussion. Energy Conversion Manag 2016;114:364–75. http://dx.doi.org/10.1016/j.enconman.2016.02.042.

[39] Bosch W. The fuel rate indicator: A new measuring instrument for display of the characteristics of individual injection. SAE Techn Pap 660749 1966. http://dx.doi.org/10.4271/660749.

[40] Payri R, Gimeno J, Martí-Aldaraví P, Vaquerizo D. Momentum flux measurements on an ECN GDi injector. In: SAE Technical Paper 2015-01-1893. 2015, p. 11. http://dx.doi.org/10.4271/2015-01-1893, URL http://papers.sae.org/2015-01-1893/.

[41] Cavicchi A, Postrioti L, Berni F, Fontanesi S, Di Gioia R. Evaluation of hole-specific injection rate based on momentum flux measurement in GDI systems. Fuel 2020;263. http://dx.doi.org/10.1016/j.fuel.2019.116657.

[42] Payri R, Bracho G, Soriano JA, Fernández-Yáñez P, Armas O. Nozzle rate of injection estimation from hole to hole momentum flux data with different fossil and renewable fuels. Fuel 2020;279:118404. http://dx.doi.org/10.1016/j.fuel.2020.118404.

[43] Shahangian N, Miyagawa J, Sharifian L, Uehara K, Noguchi Y, Payri R, Martí-aldaraví P, Bautista A, Bergamini S. Spray orientation assessment and correction method for GDI momentum flux measurements. In: "17th Conference. The working process of the internal combustion engine". Institute of Internal Combustion Engines and Thermodynamics, Graz University of Technology; 2019, p. 231–41.

[44] Du J, Chen H, Li Y, Ye L, Li G. Experimental study on ethanol gasoline flash-boiling spray characteristics using multi-hole GDI injector. In: Proceedings of china SAE congress 2019: Selected papers. Singapore: Springer Singapore; 2021, p. 635–45.

[45] Medina M, Bautista A, Wooldridge M, Payri R. The effects of injector geometry and operating conditions on spray mass, momentum and development using high-pressure gasoline. Fuel 2021;294:120468. http://dx.doi.org/10.1016/j.fuel.2021.120468.

[46] Dernotte J, Hespel C, Foucher F, Houillé S, Mounaïm-Rousselle C. Influence of physical fuel properties on the injection rate in a Diesel injector. Fuel 2012;96:153–60. http://dx.doi.org/10.1016/j.fuel.2011.11.073.

[47] Payri R, Garcia A, Domenech V, Durrett RP, Plazas AH. An experimental study of gasoline effects on injection rate, momentum flux and spray characteristics using a common rail diesel injection system. Fuel 2012;97:390–9. http://dx.doi.org/10.1016/j.fuel.2011.11.065.

[48] Cavicchi A, Postrioti L. Simultaneous needle lift and injection rate measurement for GDI fuel injectors by laser Doppler vibrometry and Zeuch method. Fuel 2021;285:119021.

[49] Bautista Rodríguez A. Study of the gasoline direct injection process under novel operating conditions. [Ph.D. thesis], Universitat Politècnica de València; 2021.